Generation and Measurement of Relativistic Electron Bunches Characterized by a Linearly Ramped Current Profile

R. J. England, J. B. Rosenzweig, and G. Travish

Department of Physics and Astronomy, University of California Los Angeles, 405 Hilgard, Los Angeles, California 90095, USA

(Received 9 January 2008; published 28 May 2008)

We report the first successful attempt to generate ultrashort (1–10 ps) relativistic electron bunches characterized by a ramped longitudinal current profile that rises linearly from head to tail and then falls sharply to zero. Bunches with this type of longitudinal shape may be applied to plasma-based accelerator schemes as an optimized drive beam, and to free-electron lasers as a means of reducing asymmetry in microbunching due to slippage. The scheme used to generate the ramped bunches employs an anisochronous dogleg beam line with nonlinear correction elements to compress a beam having an initial positive time-energy chirp. The beam current profile is measured using a deflecting mode cavity, and a pseudoreconstruction of the beam's longitudinal phase space distribution is obtained by using this diagnostic with a residual horizontal dispersion after the dogleg.

DOI: 10.1103/PhysRevLett.100.214802 PACS numbers: 41.85.Ct, 29.27.Eg, 41.85.Ew

Techniques for longitudinally compressing electron beams have long been employed as a means of obtaining higher peak current. It has been proposed in recent years that certain experimental efforts may also benefit from high-current beams that have a particular *shape* of current profile, namely, that of a triangular ramp which rises linearly from head to tail and then drops abruptly to zero. In free-electron lasers high-gain harmonic generation experiments, a prebunching undulator is used to create an energy modulation of the beam, which is then translated into spatial microbunching with a magnetic compressor. It has recently been proposed that the use of a beam with a triangularly ramped current profile may help to counteract inhomogeneity in the microbunching due to slippage [1]. In the case of the plasma wakefield accelerator (PWFA), it has been established through 1D and 2D theory as well as simulations that a triangular ramp is the optimal shape of current profile for the drive beam [2–4]. In particular, a ramped current profile maximizes the energy ΔE that can be gained by a trailing particle accelerated in the wakefield normalized to the drive beam energy E. The so-called *transformer ratio* is given by $\Delta E/E = k_p L$, where k_p is the inverse plasma skin depth and L is the length of the triangular ramp. This ratio can therefore be made arbitrarily large if k_p^{-1} is made sufficiently small relative to L. Such a scenario is illustrated in Fig. 1, which shows a ramped drive beam exciting a longitudinal wakefield E_z in order to accelerate a trailing bunch of smaller charge.

Recent experiments at Argonne National Laboratory have succeeded in producing a linearly growing *train* of bunches, and in demonstrating the resultant transformer ratio enhancement of the wakefields in a metallic structure [5]. However, no one has previously demonstrated a reliable method of generating a ramp-shaped current profile within a single short bunch. We proposed such a scheme in a previous article [6]. In the present letter we review the technique employed and present the experimental verification of it, which was obtained by using a transverse deflecting mode cavity to reconstruct the current profiles of the electron bunches with sub-ps resolution.

The method employed for generating bunches with a ramped current profile requires that an energy chirp be initially imposed upon the beam. This can be accomplished by injecting the beam into the linac cavity after the peak of the accelerating gradient. Particles at the leading edge of the beam then see a higher integrated field across the structure and emerge with higher energy than the tail particles. This process results in a correlation between longitudinal position z within the bunch and momentum p that is nonlinear, due to the sinusoidal variation of the linac accelerating gradient. This nonlinearity can be seen in the slight curvature of the longitudinal phase space distribution in Fig. 2(a). The particle distribution and current profile of Fig. 2(a) were obtained from the output of a particle-tracking simulation (using 10 000 macroparticles) of the photoinjector and linac at the UCLA Neptune laboratory, using the code PARMELA [7]. The chirp was gener-

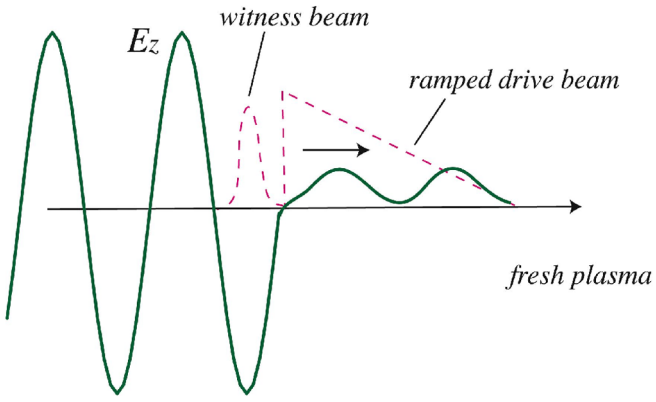

FIG. 1 (color online). Schematic illustration of the plasma wakefield accelerator with a ramped drive beam and a trailing witness bunch.

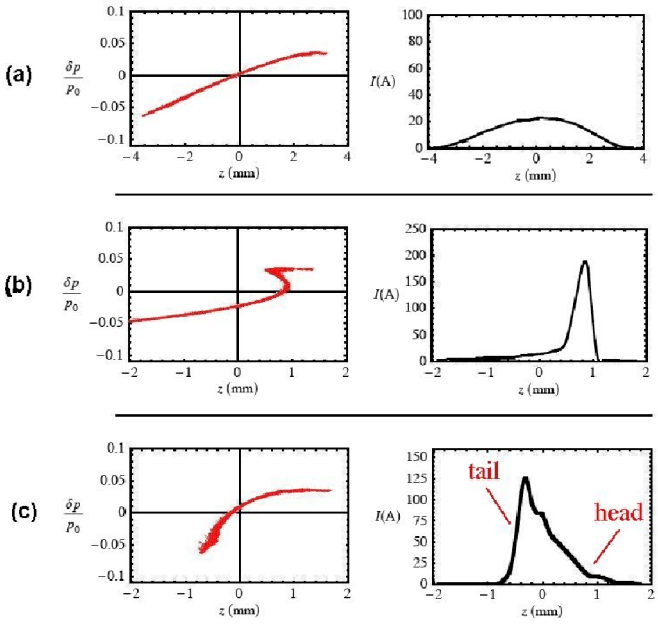

FIG. 2 (color online). Longitudinal phase space (left) and current profiles (right) for a chirped distribution (a) before manipulation, and after applying transformations that are (b) quadratic and (c) linear in the momentum error.

ated in the simulation by setting the injection rf phase of the beam in the linac section 20° behind the peak accelerating gradient.

When a beam with a positive chirp, such as that of Fig. 2(a), traverses an anisochronous beam line with a negative longitudinal dispersion, the particles at the head and tail catch up with each other due to the longer pathlength traversed by particles with a positive momentum deviation δp from the average momentum p_0 of the bunch. A simple example of such a beam line is a so-called ''dogleg'' consisting of two bending magnets with bend angles of equal magnitude but opposite sign separated by a straight section (labeled ''Dogleg Compressor'' in Fig. 3). Symmetrically placed (magnetic quadrupole) lenses in the straight section ensure, to first order in a perturbative expansion in powers of $\delta \equiv \delta p/p_0 \ll 1$, that particles of different energy which enter the device collinearly, are collinear upon exiting as well.

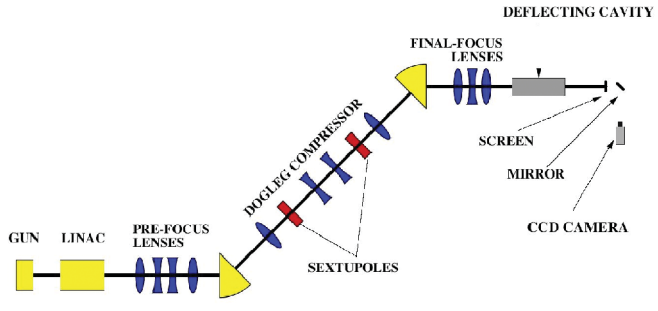

FIG. 3 (color). Cartoon of the experimental beam line with bending magnets, quadrupole focusing magnets, and sextupole correctors marked by yellow wedges, blue lenses, and red rectangles, respectively.

It was found in Ref. [6] that for such a device, the compression is approximately characterized by the following transformation of the longitudinal (z) coordinates of the particles, expressed relative to the bunch center:

$$z_f = z_0 + \eta_z \delta + \tau_z \delta^2. \quad (1)$$

Here z_0 and z_f are the initial and final longitudinal positions of a given particle. The coefficients η_z and τ_z are the first- and second-order *longitudinal dispersion* terms, respectively. This expression is valid when the beam rms size and angles (σ_x, σ_θ) are well constrained (i.e., $\sigma_x \ll \eta_z$ and $\sigma_\theta \ll \eta_z/\tau_z$). Higher-order terms proportional to δ^3, δ^4, etc., which are omitted in Eq. (1), may also be significant in some cases, as discussed in Ref. [6].

In Fig. 2(b) the simple transformation of Eq. (1) has been applied to each of the macroparticles in Fig. 2(a), producing a new phase space distribution whose current profile appears as a sharp spike followed by a trailing tail. The values used for η_z and τ_z are those predicted by simulations and analytical formulas for the dogleg shown in Fig. 3. If the second-order coefficient τ_z is set to zero, however, the transformation becomes purely linear, and the transformed phase space distribution appears as in Fig. 2(c). Here the curvature of the distribution in Fig. 2(a) has now been linearly magnified by the compression, producing a hook-shaped distribution, corresponding to a nearly triangular current profile. The elimination of τ_z is accomplished by the inclusion of a pair of sextupole corrector magnets on the dogleg (marked in Fig. 3). Proper placement of the sextupoles near the horizontally focusing lenses and calculation of the values η_z and τ_z are discussed in Ref. [6]. The two sextupoles are operated with equal field magnitude but with opposite polarity.

Although the manipulations used in Figs. 2(b) and 2(c) are governed only by the simple transformation of Eq. (1), the resulting shapes of the longitudinal phase space distributions and current profiles are almost identical to those which were obtained using sophisticated particle-tracking codes (see Fig. 3 of Ref. [6]). This agreement indicates that Eq. (1) reasonably models the transformation we are describing.

The relevant aspects of the experimental setup for generating ramp-shaped bunches at the UCLA Neptune laboratory is illustrated in Fig. 3. High-brightness 300 to 600 pC bunches of 4 MeV electrons are generated by the photoinjector gun and accelerated in the linac to near 13 MeV, with injection into the linac performed 20° after the rf crest in order to produce the required energy chirp. After passing through the dogleg, which imparts a transformation of the form in Eq. (1), the beam is focused by a triplet of quadrupole magnets through the deflecting cavity aperture and onto a profile imaging screen. A Faraday cup at the location of the screen can be inserted into the beam path to measure the beam's charge.

The deflecting cavity is a purpose-built 9-cell standing wave structure driven at 9.596 16 GHz (an integer multiple

of the 38.08 MHz drive laser oscillator frequency of which the 2.856 GHz gun and linac rf is also a multiple, thereby insuring relative phase stability) with a maximum deflecting voltage V_0 in the vertical (y) direction of up to 500 kV at 50 kW of input power. The deflector design is discussed in detail in Ref. [8]. The achievable temporal resolution of this diagnostic is limited by the minimum spot size σ_0 that is achieved on the downstream imaging screen when $V_0 = 0$. This can be seen from the relation between a particle's longitudinal position z within the beam and its vertical position y on the deflector screen,

$$y = y_0 + \frac{eV_0L}{p_0c}(\sin\phi + kz\cos\phi). \quad (2)$$

Here y_0 is the particle's position with the deflector off, V_0 is the cavity voltage, L is the drift length to the screen, p_0 is the mean momentum, ϕ is the beam's mean injection phase, c is the speed of light, e is the electron charge, z is related to arrival time t by $z = c(t_0 - t)$, where t_0 is the arrival time of the bunch center, and k is the rf wave number. If one wishes to reconstruct the time dependence of the beam current profile using Eq. (2) the spread in values $\sigma_0 = \langle y_0 \rangle$ must be negligible, which implies an achievable time resolution of $\Delta t = \sigma_0 p_0/(kLeV_0)$. For the parameter values in Table I and $\sigma_0 = 200$ μm this gives a resolution of ~400 fs for the present experiment.

The deflecting voltage produced by the cavity was benchmarked by varying ϕ away from zero and observing the resultant deflection of the beam centroid. The benchmarking was done at a reduced power level of 12 kW to prevent the beam from being deflected off of the imaging screen at $\phi = 90°$. The deflecting voltage was then extracted from a sinusoidal fit to Eq. (2), yielding $V_0 = 232 \pm 9.6$ kV at this power level. The deflecting voltage at other power (P) levels was calibrated through this level, noting that $V_0 \propto P^{1/2}$.

Prior to running a chirped beam through the dogleg and the deflector, the beam was run near the linac phase for minimum momentum spread, in order to optimize the transport and measure the longitudinal structure of the uncompressed pulse. An example trace of the deflector streak produced under these conditions is shown in Fig. 4. In this example, the beam energy was 13 MeV and the measured beam charge Q was 270 pC.

The image in Fig. 4(a) shows the focused beam with the deflecting cavity turned off. When the deflecting cavity is turned on at an input power of 41 kW the beam is streaked along the vertical axis producing the image in (b). The contour plots in parts (a) and (b) of Fig. 4 are false-color reconstructions of the captured black-and-white CCD camera images of the profile screen. The images were processed using 5×5 pixel binning, interpolation, and background subtraction.

The plot in Fig. 4(c) shows the reconstructed current profile based upon the streaked image in part (b) and the measured value of Q. We see from this plot that there is an asymmetry in the uncompressed pulse, with greater charge at the head. This structure may be attributed to structure in the drive laser pulse combined with longitudinal space-charge effects. The rms bunch length of the current distribution in Fig. 4(c) is approximately 6 ps, which is consistent with optical measurements of the photocathode drive laser pulse length.

Deflecting cavity data for an electron beam that was chirped in momentum by running the rf phase in the linac backward of crest by 20° are shown in Fig. 5. Experimental parameters corresponding to the data of Fig. 5 are shown in Table I. As seen in Fig. 5(a), when the normalized sextupole magnetic field strength (defined by $\kappa = (e/p_0c) \times (\partial^2 B_y/\partial x^2)$, where B_y is the vertical field component) is set to zero, the profile is characterized by a sharp narrow spike at the head, followed by a shallow tail, as was seen in Fig. 2(b). As the sextupole strength is increased, the hard edge at the head of the beam gives way to a gradual ramp followed by a sharp drop at the tail seen in Fig. 5(e). The intermediate stages shown in (b) through (d) demonstrate the progression of this process. In these streaks, the first quadrupole lens on the dogleg was detuned, producing a slight correlation between x and δ having both linear and higher-order contributions. As the linear correlation is dominant, the streak images show a pseudoreconstruction of the longitudinal phase space with an energy correlation on the x axis (shown as vertical) and time on the y axis (shown as horizontal). The progression from (a) to (e) therefore empirically demonstrates the "turning over" of the phase space distribution with increasing sextupole strength predicted by simulation in Ref. [6].

The sextupole field strength ($\kappa = 2188$ m^{-3}) required to produce the ramp-shaped beam in Fig. 5(e) is 80%

TABLE I. Experimental parameters.

Parameter	Value	Units
Beam energy (p_0c)	11.8	MeV
rf frequency of Gun and Linac	2.856	GHz
rf frequency of Deflector	9.596 16	GHz
Final beam charge (Q)	235	pC
Deflecting voltage (V_0)	400	kV
Drift length (L)	28	cm

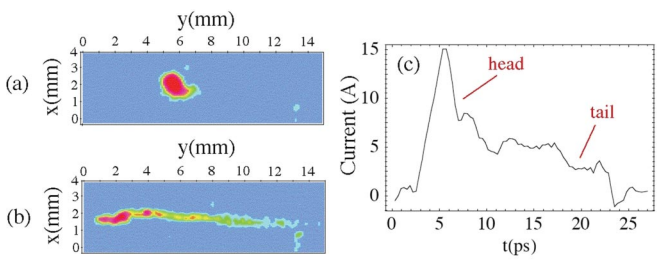

FIG. 4 (color). Deflecting cavity streaks of uncompressed electron beam with (a) deflecting cavity turned off, (b) deflecting cavity turned on, as well as (c) the current profile reconstruction of the image in part (b).

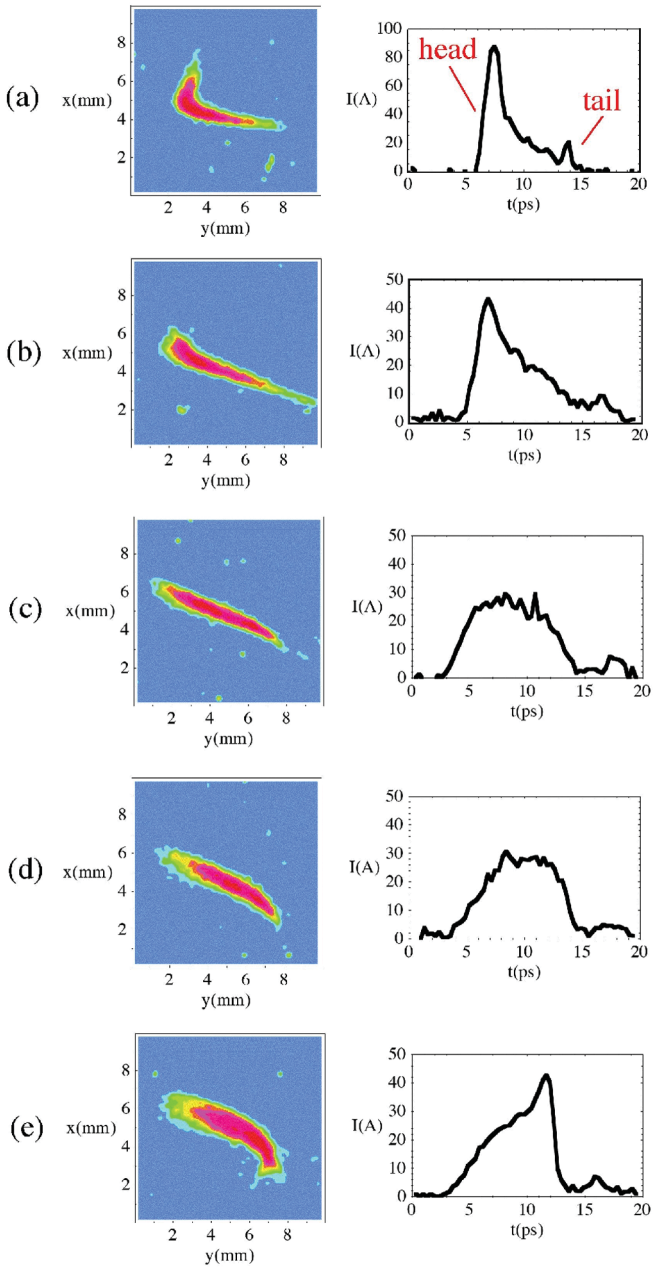

FIG. 5 (color). Deflecting cavity streaks (left) and current profile reconstructions (right) of an initially chirped electron beam for five different sextupole field values: (a) $\kappa = 0$, (b) $\kappa = 547\ \mathrm{m}^{-3}$, (c) $\kappa = 1094\ \mathrm{m}^{-3}$, (d) $\kappa = 1641\ \mathrm{m}^{-3}$, and (e) $\kappa = 2188\ \mathrm{m}^{-3}$.

higher than what was predicted by the simulations and empirical measurements of Ref. [6] to be necessary to cancel the second-order coefficient τ_z in Eq. (1). Consequently, the ramped beam of Fig. 5(e) is characterized by a significant overcorrection of the second-order longitudinal dispersion. This overcorrection is most likely required by the fact that the uncompressed bunches (as illustrated in Fig. 4) are not Gaussian but are asymmetric with higher current at the head than the tail. By using a simulated input beam with a similar asymmetry in the current profile and overcompensating the sextupoles in the simulation by 80%, the main features of the hook-shaped streak image and triangular profile in Fig. 5(e) have indeed been reproduced using the particle-tracking code ELEGANT [9].

In summary, we have experimentally verified the proposed technique for generating triangularly ramped electron bunches, by employing a high-frequency transverse deflecting cavity to reconstruct the current profiles of the electron beam. Because of the asymmetric longitudinal structure of the initial electron bunch (before the compression), production of ramped bunches was found to require a higher degree of sextupole field correction than what was previously predicted for initially Gaussian bunches [6]. This observation indicates that the bunch-ramping mechanism is somewhat forgiving of such asymmetries, since ramped bunches can be obtained in spite of them by adjusting the strength of the sextupoles. In future measurements at Neptune, this type of ramped beam pulse will be deployed in experiments leading to investigations of high transformer ratio PWFA.

Work supported by U.S. DOE Grant No. DE-FG03-92ER40693.

[1] C. Sung, S. Y. Tochitsky, S. Reiche, J. B. Rosenzweig, C. Pellegrini, and C. Joshi, Phys. Rev. ST Accel. Beams **9**, 120703 (2006).
[2] K. L. F. Bane, P. Chen, and P. B. Wilson, SLAC Tech. Report No. SLACPUB-3662, Stanford Linear Accelerator Center, Stanford, CA, 1985.
[3] J. B. Rosenzweig, Phys. Rev. A **44**, R6189 (1991).
[4] K. V. Lotov, Phys. Plasmas **12**, 053105 (2005).
[5] C. Jing, A. Kanareykin, J. G. Power, M. Conde, Z. Yusof, P. Schoessow, and W. Gai, Phys. Rev. Lett. **98**, 144801 (2007).
[6] R. J. England, J. B. Rosenzweig, G. Andonian, P. Musumeci, G. Travish, and R. Yoder, Phys. Rev. ST Accel. Beams **8**, 012801 (2005).
[7] L. Young and J. Billen, LANL Tech. Report No. LA-UR-96-1835, Los Alamos National Laboratory, Los Alamos, NM, 1996.
[8] R. J. England, D. Alesini, B. O'Shea, J. B. Rosenzweig, and G. Travish, in *Proceedings of the 2006 Advanced Accelerator Concepts Workshop*, AIP Conference Proceedings No. 877 (AIP, New York, 2006), p. 595.
[9] M. Borland, Tech. Report No. LS-287, Argonne National Laboratory Advanced Photon Source, Argonne, IL, 2000.